Supplementary Information

Ultra-thin graphene-polymer heterostructure membranes

*Christian Berger, Marian Dirschka and Aravind Vijayaraghavan**

Supplementary Discussion S1: Effective elastic properties of graphene-polymer heterostructures

Assuming that heterostructure membranes are fully clamped around the edges of the micro-cavity and exhibit a negligible Poisson effect, the biaxial modulus is given by the Voigt upper bound mixing rule $E_{\mathrm{Voigt}} = E_{\mathrm{g}}\phi_{\mathrm{g}} + E_{\mathrm{p}}\phi_{\mathrm{p}}$, where ϕ_{g} and ϕ_{p} are the volume fractions of the graphene and the polymer respectively[1].

We validate the first assumption by directly measuring a sharp drop in the out-of-plane Derjaguin-Muller-Toporov modulus of the membranes at the membrane-substrate delamination front as we move from the supported to the suspended section. This measurement was taken using the PeaForce™ Quantitative Nanomechanical Mapping mode on a Bruker FastScan AFM[2]. With regards to the second assumption we assume the Poisson effect to have a negligible influence on the effective biaxial modulus, as even for a two layered composite where the constituent phases of Poisson ratio $\nu_{\mathrm{A}} = 0$, $\nu_{\mathrm{B}} = 0.5$ and elastic modulus ratio $\frac{E_{\mathrm{B}}}{E_{\mathrm{A}}} = 1$ gives a ratio of the actual modulus to its upper bound, $\frac{E_{\mathrm{AB}}}{E_{\mathrm{Voigt}}} = 1.103$ [1]. Therefore the modified elastic modulus of the graphene-polymer heterostructure membrane is given by

$$S = \frac{1}{1-\nu_{\mathrm{eff}}}\left(E_{\mathrm{p}}t + E_{\mathrm{2d-g}}\right) = \frac{E_{\mathrm{p}}t}{1-\nu(t)}(1+\lambda) \tag{1}$$

where E_{p} is the bulk Young's modulus of the polymer, $E_{\mathrm{2d-g}}$ is the two-dimensional Young's modulus of graphene $\lambda = \frac{E_{\mathrm{2d-g}}}{E_{\mathrm{p}}}$ and ν_{eff} is the effective Poisson ratio dependent on the volume fraction ratio of the heterostructure composite. Similarly to above, the effective bending stiffness and effective Poisson's ratio is given by

$$D = \frac{E_{\mathrm{p}}t^3}{12(1-\nu_{\mathrm{eff}})}\frac{1+4\lambda}{1+\lambda} \tag{2}$$

$$\nu_{\mathrm{eff}} = \nu_{\mathrm{p}}\left(1 - E_{\mathrm{g}}\phi_{\mathrm{g}}\right) + \nu_{\mathrm{g}}\left(1 - E_{\mathrm{p}}\phi_{\mathrm{p}}\right) \tag{3}$$

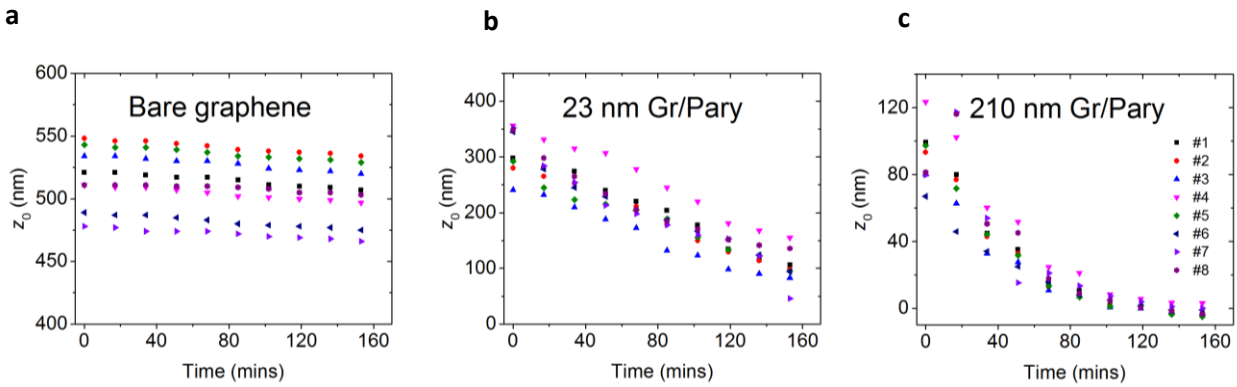

Supplementary Figure S1: Nitrogen gas leakage from micro-blisters. (**a - c**) The maximum deflection point z_0 of individual bare graphene membranes and 23 nm and 210 nm graphene-polymer membranes is plotted in 17 minute time intervals for a total of 153 minutes after pumping all samples to 400 kPa. Eight different membranes (#1-8) are plotted for each thickness.

Supplementary Discussion S2: Leakage rate and air-tightness of membranes

In order to characterise the leakage rate of membranes, we monitored the change in deflection of the membranes over time after pressurisation. Each of the membranes measured in the micro-blister experiment was pressurised to 400 kPa with nitrogen gas using the micro-blister inflation method described in the main article. We then measured the height profile of the deflected membranes in 17 minute intervals over 3 hours using ScanAsyst^{TM} AFM imaging mode. The time scale of complete deflation from 400 kPa for bare graphene, 23 nm and 210 nm graphene-polymer heterostructure membranes is approximately 22, 6 and 2 hrs respectively. The time of removal from the pressure chamber is between -5 to -10 minutes in reference to the figure. We obtain the leak rate, $\delta z/\delta t$ from this plot in order to estimate the deflection at the time of removal from the pressure chamber. This correction is then applied to all deflection values measured throughout the micro-blister experiment.

The time interval between removing samples from the pressure chamber and measuring the membrane is typically kept below 10 minutes. For bare graphene and 20 nm graphene-polymer samples this period results in a negligible change in deflection, however, 100 nm and 200 nm thick membranes show a drop of 3% and 5% in deflection giving rise to an increased error in the effective deflection. The sharp increase in gas leakage with membrane thickness is attributed to an increase in bending rigidity of the membranes, reducing the ability for the membrane to conform to the substrate to form a gas tight seal. Gas leakage directly through the membrane is considered negligible as this effect is expected to show the opposite trend in deflation rate as a function of thickness.

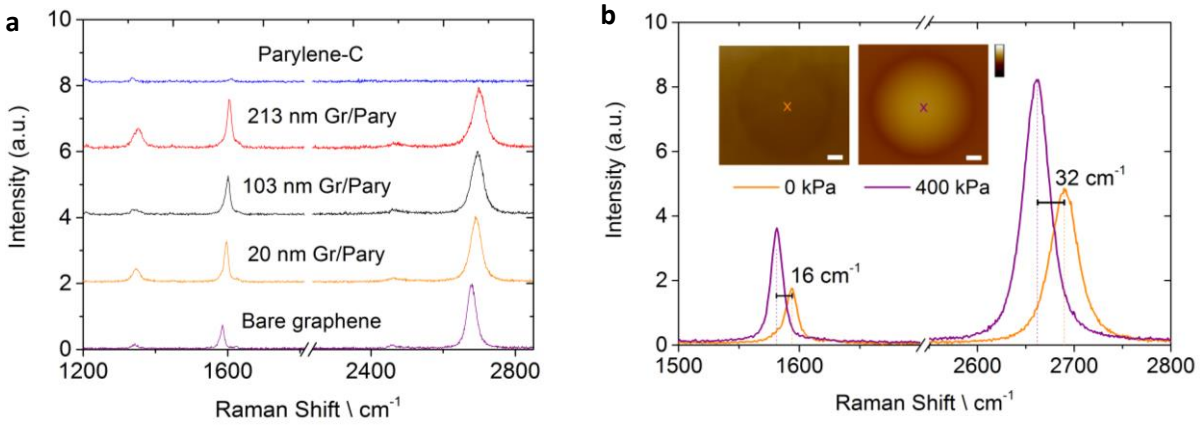

Supplementary Figure S2: The Raman spectrum of graphene-polymer heterostructures. (**a**) The Raman spectra of bare graphene, Parylene-C, 20 nm, 103 nm and 213nm graphene-polymer heterostructures. The signal intensities are normalised to the 2D peak intensity. (**b**) The Raman spectra in the region of the G and 2D peak taken at the centre of a 6 µm diameter, 102 nm thick graphene-polymer membrane at 0kPa and 50kPa. Scale bars: 1.5 µm, 0 nm - 400 nm.

Supplementary Discussion S3: Raman spectral analysis of heterostructure membranes

The Raman spectra of four different thicknesses of bare graphene and graphene-polymer heterostructures supported on Si/SiO_2 substrates were measured at an excitation energy of 2.4eV (514 nm) using an inVia^{TM} Renishaw confocal microscope. The spectrum for all four thicknesses is representative of single-layer CVD graphene, with a distinctive G and 2D peak at around 1580 and 2680 cm^{-1} respectively. On increasing the thickness of polymer, we observe a drop in the intensity ratio between the G and the 2D peak as well as emerging of the D peak (1340 cm^{-1})[3]. This is suggestive of some defects in the graphene layer, however, previous reports on bare single-layer CVD graphene have shown a similar degree of defects whilst demonstrating the same superior mechanical characteristics of pristine graphene[4]. Thus, we assume that the deposition of Parylene-C has negligible effect on the structural integrity of the graphene layer. In addition we did not observe any significant shift in the G or 2D peak as a function of polymer thickness, which is consistent with previous measurements[5].

In order to confirm the strain transfer between the graphene and polymer layers, we compare the Raman spectrum at the centre of a 102 nm membrane at equilibrium (P=0 kPa) and when pressurised. At a pressure of 400 kPa we determine a strain of $0.22\pm0.4\%$ in the suspended region of the membrane from the shift in the G and 2D peak shift[6,7]. This value is comparable to the strain measured by the micro-blister inflation study (0.24%) and thereby confirms effective strain transfer between the graphene and the polymer layer.

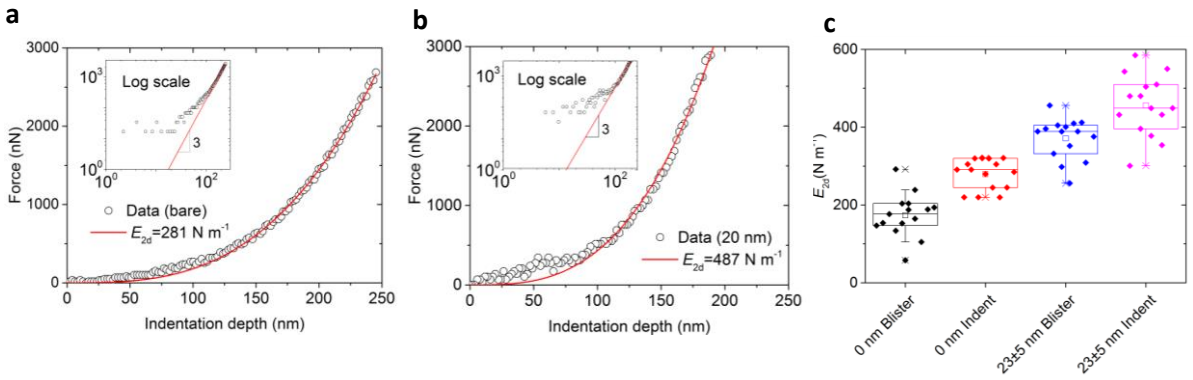

Supplementary Figure S3: Comparison of elastic modulus obtained by blister test and nanoindentation. a) Force-distance curve of a single nanoindentation on a bare suspended graphene membrane and **b)** of a 20nm thick heterostructure membrane respectively. **c)** A box chart summarises the in-plane stiffness measured by the micro-blister inflation and nanoindentation experiment.

Depositing the graphene-Parylene-C heterostructure onto a blank substrate ensures that any undulations from the copper foil, which the graphene was initially grown on, are flattened out. This also allows us to pattern graphene without modifying the Parylene-C layer due to plasma etching[8]. The graphene-polymer stack is then removed from the substrate using diluted potassium hydroxide and is cleaned and dried in preparation for transfer. On a separate substrate, the TLM electrode structure is defined using a photomask followed by thermal evaporation of a 2 nm/50 nm chromium/gold stack. The resist is then cleaned off with acetone and the substrate is plasma cleaned before transfer (2B ii). We accurately align the patterned graphene-polymer membrane with the TLM electrodes using an custom-made transfer system (2B iii) and proceed with the same transfer steps as for the micro-blister structure (2B iv-v).

Supplementary Discussion S5: Elastic modulus measurements by nano-indentation

AFM nanoindentation measurements were carried out on the same bare graphene and 20nm membranes as used in the micro-blister inflation experiments in order to cross-check the 2d in-plane modulus measured[9]. This point is then indented using a Bruker DDESP-10 diamond tip to measure the ramp distance, z and cantilever deflections, δ. Prior to measurement the cantilever spring constant (80 Nm^{-1}) and deflection sensitivity were calibrated by thermal tuning and indenting the tip on a diamond reference sample respectively. First we located the centre of each membrane using PeakForce^{TM} imaging mode[2]. Force-indentation curves were obtained as $F = -k\delta$ and $h = z - \delta$. The 2d in-plane modulus, $E_{2\mathrm{d}}$ was then extracted by fitting the nanoindentation equation[10],

$$F = \sigma_0 \pi h + \frac{E_{2\mathrm{d}} q^3 h^3}{a^2} \qquad (1)$$

where a is the membrane radius and constant q=1.02 is related to the Poisson's ratio of graphene. We conducted indentations at the equivalent force to that applied in the micro-blister experiment (200 nN - 1000 nN) and found consistency in the 2d in-plane modulus with a value of $E_{2\mathrm{d}}$ =158±20 Nm^{-1}. We noticed that choosing the correct zero-point deflection, *zdp* ($z = 0$) is critical in obtaining an accurate in-plane modulus; A shift in the *zdp*

by just 5 nm showed a difference in the 2d in-plane modulus of up to 50 Nm^{-1}. Due to the intrinsic crumpling of suspended CVD graphene the *zpd* can vary by up to 10 nm thereby increasing the effective error by up to 70 Nm^{-1}. By applying larger forces, this inaccuracy becomes less prominent as the *zdp* has less influence. We also measured the same membranes as in the micro-blister experiments with higher forces (<3000 nN), obtaining a 2d in-plane modulus closer to that given in literature (345 Nm^{-1})[9]. Similar observations were made for heterostructure membranes with thicknesses of 23±5 nm. Typical force curves obtained when indenting at higher forces are shown in Supplementary Fig. 4a and 4b. We note here that the pronounced intrinsic crumpling of the 20 nm membranes skews the fitting of the force curve, giving a large error in the extracted modulus as shown in Supplementary Fig. 4c. In addition, the forces required to achieve a significant membrane deflection in thicker membranes extends beyond the range regarded as safe for the diamond AFM tip and cantilever. Hence, our AFM studies were limited to measurements of bare and 20 nm thick membranes only. We note here that the initial fabrication process included critical point drying of the membranes instead of rinsing in hexane as the final step. We eliminated this step as this process exerts over 100 MPa on the devices, resulting in membrane strains beyond the elastic limit. However, we noticed a negligible difference in the membrane yield using this process, confirming that the ultimate tensile strength of almost all membranes is above 100 MPa.

Supplementary Discussion S6: Slippage at high loadings

An indication of slip is characterised by a drop in the stress of inflated membranes at high strains. We applied high pressures to two membranes in order to determine an approximate critical strain for slipping, ϵ_c as shown in Figure S4. Slippage is observed in two individual samples with membrane thickness of 20 nm and 19 nm respectively. For analysis of the elastic properties of membranes we applied pressures so that membranes would be probed below this critical strain.

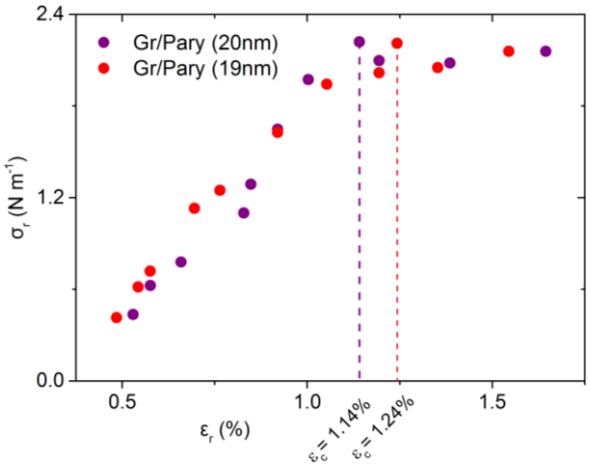

Supplementary Figure S4. Stress-strain plot for two 5 µm diameter membranes pressurised to 600 kPa demonstrates slippage artefacts at 1.14% and 1.24% strain for each of the probed membranes.

Supplementary Discussion S7: Thickness of graphene-polymer films

The error in our thickness measurements is determined by calculating the standard deviation of an AFM height trace at least 15 µm from a torn edge. For example the calculated error from Figure S5 c and d is 1.3 nm and 1.5 nm respectively.

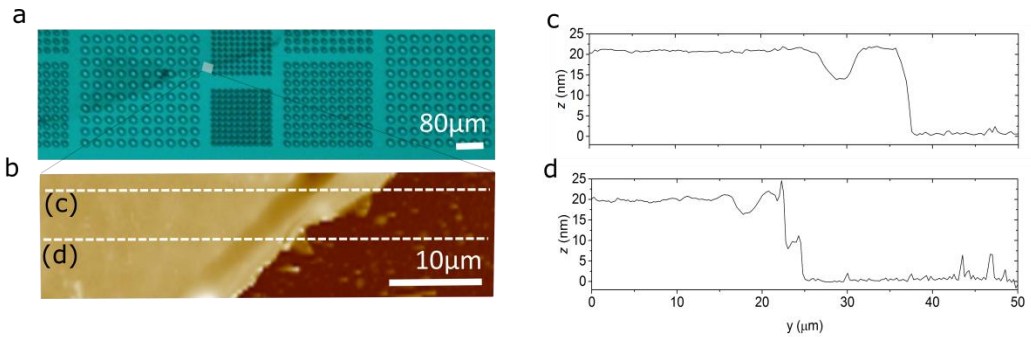

Supplementary Figure S5 (a) Optical micrograph of a sample with the graphene-Parylene-C layer partially removed for thickness measurement. **(b)** An AFM height map of the small grey square in Figure S6a. The two dashed white lines indicate two traces that are plotted in the following figures. **(c)** The top and **(d)** bottom height trace in Figure S6b.

Supplementary References

1. Liu, B., Feng, X. & Zhang, S.-M. The effective Young's modulus of composites beyond the Voigt estimation due to the Poisson effect. *Composites Science and Technology* **69,** 2198–2204 (2009).

2. Dokukin, M. E. & Sokolov, I. Quantitative Mapping of the Elastic Modulus of Soft Materials with HarmoniX and PeakForce QNM AFM Modes. *Langmuir* **28,** 16060–16071 (2012).

3. Eckmann, A., Felten, A., Verzhbitskiy, I., Davey, R. & Casiraghi, C. Raman study on defective graphene: Effect of the excitation energy, type, and amount of defects. *Physical Review B* **88,** 035426 (2013).

4. Rasool, H. I., Ophus, C., Klug, W. S., Zettl, a. & Gimzewski, J. K. Measurement of the intrinsic strength of crystalline and polycrystalline graphene. *Nature Communications* **4,** 1–7 (2013).

5. Mordi, G. *et al.* Low-κ organic layer as a top gate dielectric for graphene field effect transistors. *Applied Physics Letters* **100,** 193117 (2012).

6. Cao, Z. *et al.* A blister test for interfacial adhesion of large-scale transferred graphene. *Carbon* **69,** 390–400 (2014).

7. Zabel, J. *et al.* Raman Spectroscopy of Graphene and Bilayer under Biaxial Strain: Bubbles and Balloons. *Nano Letters* **12,** 617–621 (2012).

8. Oehrlein, G. S., Phaneuf, R. J. & Graves, D. B. Plasma-polymer interactions: A review of progress in understanding polymer resist mask durability during plasma etching for nanoscale fabrication. *Journal of Vacuum Science & Technology B: Microelectronics and Nanometer Structures* **29,** 010801 (2011).

9. Lee, G.-H. *et al.* High-Strength Chemical-Vapor-Deposited Graphene and Grain Boundaries. *Science* **340,** 1073–1076 (2013).

10. Tan, X. *et al.* Nanoindentation models and Young's modulus of monolayer graphene: A molecular dynamics study. *Applied Physics Letters* **102,** 071908 (2013).